A Noise-Reduced Light-to-Frequency Converter for Sub-0.1% Perfusion Index Blood SpO₂ Sensing

Fang Tang , *Senior Member, IEEE*, Zhipeng Li , Tongbei Yang, Lai Zhang, Xichuan Zhou , Shengdong Hu, Zhi Lin , Ping Li , Bo Wang , *Member, IEEE*, and Amine Bermak , *Fellow, IEEE*

Abstract—To improve the SpO₂ sensing system performance for hypoperfusion (low perfusion index) applications, this paper proposes a low-noise light-to-frequency converter scheme from two aspects. First, a low-noise photocurrent buffer is proposed by reducing the amplifier noise floor with a transconductance-boost (g_m-boost) circuit structure. Second, a digital processing unit of pulse-frequency-duty-cycle modulation is proposed to minimize the quantization noise in the following timer by limiting the maximum output frequency. The proposed light-to-frequency sensor chip is designed and fabricated with a 0.35-μm CMOS process. The overall chip area is 1 × 0.9 mm² and the typical total current consumption is about 1.8 mA from a 3.3-V power supply at room temperature. The measurement results prove the proposed functionality of output pulse duty cycle modulation, while the SNR of a typical 10-kHz output frequency is 59 dB with about 9-dB improvement when compared with the previous design. Among them, 2–3 dB SNR improvement stems from the gm-boosting and the rest comes from the layout design. In-system experimental results show that the minimum measurable PI using the proposed blood SpO₂ sensor could be as low as 0.06% with 2-percentage-point error of SpO₂. The proposed chip is suitable for portable low-power high-performance blood oximeter devices especially for hypoperfusion applications.

Index Terms—Blood SpO₂, low noise, hypoperfusion, light-to-frequency converter, portable biomedical sensor.

I. INTRODUCTION

BLOOD oximeter can detect blood oxygen saturation (SpO₂), perfusion index (PI), pulse rate (PR) and other respiratory parameters in a non-invasive, real-time manner, providing a direct and effective information for clinical anesthesia, infant monitoring and intensive care [1]. The measurement of SpO₂ using blood oximeter is based on Beer-Lambert law of vascular tissue when it is transilluminated by narrow-wavelength lights, which is dependent on the different absorption ratio in red and infrared lights [2]. Perfusion Index shows the ratio between DC and AC blood SpO₂ signals, which reflects the vascular pulse intensity [3]. For normal human bodies, perfusion index is 3% to 10%, however in clinical applications, for elders, infants and critical patients with respiratory diseases, the blood perfusion index often shows too low (lower than 0.5%) to be accurately monitored. Moreover, different finger size and skin color can also affect the light transmittance and eventually reduce the signal-to-noise ratio (SNR) [5]. From the perspective of light propagation scheme, oximeter can be implemented with two different modes: reflection mode and transillumination mode. Reflection mode SpO₂ sensor is widely used for wearable devices such as sports bracelet associated with compensations of motion artifacts and ambient light [4], however the sensing accuracy is difficult to satisfy the requirement of medical level. Overall, there are several mainstream data conversion techniques for SpO₂ sensing in transillumination mode. The first one requires a high-resolution $\Sigma\Delta$ ADC to convert the input analog signals and directly outputs the digital value [6]. Secondly, successive-approximation-register (SAR) ADC is a promising solution for low-power applications, when high dynamic range with limited chip area is realized. In order to avoid using the large chip area $\Sigma\Delta$ ADC or SAR ADC, the third technique was proposed by using a light-to-frequency converter chip [7], where the sensed photocurrent is modulated using on-chip photodiode array and switch-capacitor analog circuit, as a result the output oscillation frequency becomes proportional to the light intensity [8]. Due to lower price, the second scheme is widely adopted in portable blood oximeters [9]. However, the light-to-frequency converter suffers from poor SNR when compared with $\Sigma\Delta$ ADC, which limits its clinical applications such as infant monitoring [10]. Moreover, the pulse frequency quantization noise in the following MCU is also limited by the timer clock speed, which is not analyzed in the previous research works and especially becomes important for ultra-low-power portable oximeters with low-frequency MCUs. Overall, the key is to improve the noise performance of the light-to-frequency converter to cover more hypoperfusion application regions.

Fang Tang, Zhipeng Li, Tongbei Yang, Xichuan Zhou, Shengdong Hu, Zhi Lin, and Ping Li are with Chongqing Engineering Laboratory of High Performance Integrated Circuits, School of Microelectronics and Communication Engineering, Chongqing University, Chongqing 400044, China (e-mail: frankfangtang@gmail.com; 799151549@qq.com; 2892921581@qq.com; zxc@cqu.edu.cn; husd@cqu.edu.cn; linzhi@cqu.edu.cn; lipingstu@cqu.edu.cn).

Lai Zhang is with Guangdong Biolight Meditech Co., Ltd., Zhuhai 519085, China (e-mail: zlbeck@126.com).

Bo Wang and Amine Bermak are with the College of Science and Engineering, Hamad Bin Khalifa University, Doha 34110, Qatar (e-mail: bwang@hbku.edu.qa; abermak@hbku.edu.qa).

Color versions of one or more of the figures in this article are available online at https://ieeexplore.ieee.org.

Digital Object Identifier 10.1109/TBCAS.2020.3010362

In this paper, a low-noise light-to-frequency converter chip is proposed, which can improve the performance of SpO$_2$ sensing systems targeted for low-PI conditions. On one hand, in order to reduce the noise of the current buffer, a transconductance-boost (g_m-boost) scheme is proposed without changing the DC operating point of the amplifier. On the other hand, in order to minimize the quantization noise due to the limited timer clock frequency, a pulse-frequency-duty-cycle-modulation digital circuit is proposed to reduce the maximum output frequency. The proposed sensor chip is fabricated using a 0.35-μm CMOS process, which shows a 9-dB SNR improvement as well as additional noise reduction due to the introduced duty-cycle modulation. In-system experimental results show that SpO$_2$ can be sensed under 0.06% PI condition within 2-percentage-point error, which is significantly improved compared with 0.2% PI condition in our previously reported design [16].

The remainder of this paper is organized as follows: Section II describes the noise sources in a typical light-to-frequency converter system. Section III proposes the low-noise output pulse-frequency-duty-cycle modulation Scheme. Section IV presents the measurement specifications of the proposed light-to-frequency converter chip, as well as the blood SpO$_2$ sensing system measurement results using the proposed low-noise chip for hypoperfusion conditions, followed by the conclusion.

II. NOISE SOURCES IN LIGHT-TO-FREQUENCY CONVERTER SYSTEM

A. System Description of Blood Oximeter Based on Light-to-Frequency Converter

Medical-grade fingertip oximeter is usually performed in transillumination mode. In such case, light is transmitted directly through the finger tissue, and a blood SpO$_2$ sensor receives light on the other side [11]. This method relies on the difference in the absorption ratio between oxyhemoglobin and deoxyhemoglobin at two wavelengths of typical 660 nm (red) and 905 nm (infrared) [12]. In practice, an oximeter device can make rapid SpO$_2$ measurement by frequently switching these two LED light sources at kHz rate [13]. Fig. 1 shows the architecture of a typical blood SpO$_2$ sensor based on a light-to-frequency converter chip and the basic operating timing diagram, which consists of a photodiode array and a current-to-frequency converter. The photodiode array is able to generate a more than 100-dB high dynamic range photocurrent, which is proportional to the intensity of incident light [14]. Then, the current-to-frequency converter integrates the photocurrent into a voltage signal, which is eventually converted into a pulse frequency waveform. The output voltage F_{osc} is a square-wave frequency signal, which can be directly quantized by a high-frequency timer in the following microcontroller (MCU) for SpO$_2$ calculation.

The typical light-to-frequency converter chip mainly consists of three parts. First, a low leakage photocurrent buffer with a photodiode generates the photocurrent I_{ph} and the leakage current I_{leak} which flow into the switched-capacitor integrator circuit. In the second part, the output voltage V_{slope} of the integrator is initially lower than the reference voltage V_{ref3},
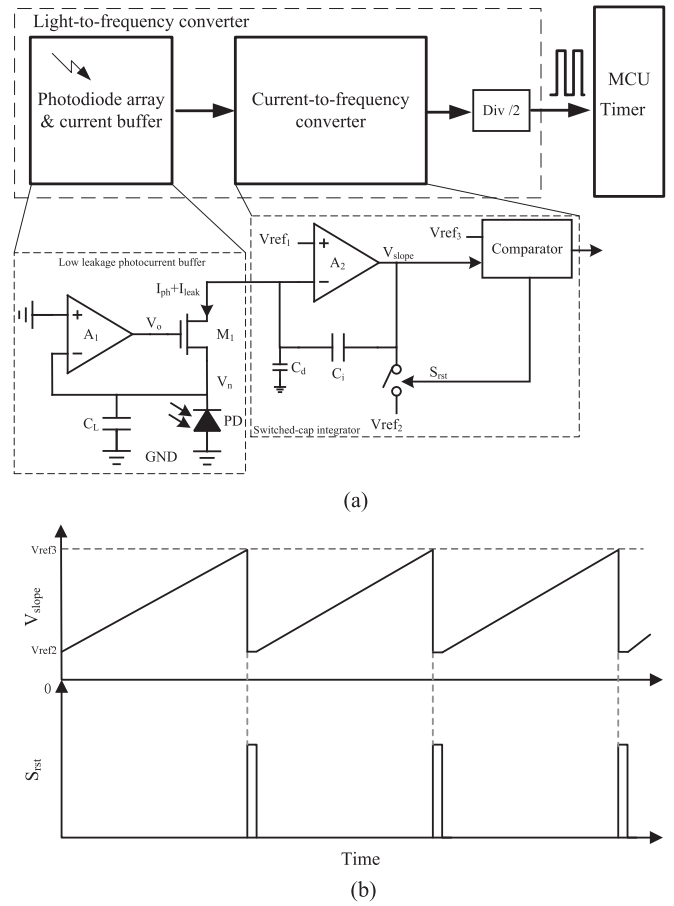

Fig. 1.   Chip architecture of a typical light-to-frequency generator (a) and the operating timing diagram (b).

and then the reset control signal S_{rst} is off. As the capacitor is continuously charged, when V_{slope} exceeds to V_{ref3}, the comparator enables S_{rst} to force V_{slope} down to the reference voltage V_{ref2}. Then, the integrating capacitor C_i starts charging again until the next reference voltage approaching. In the third part, the output frequency, inversely proportional to $V_{ref3}-V_{ref2}$, is obtained by the D-flip-flop-based /2 frequency divider with a 50% duty cycle. A de-coupling capacitor C_d is adopted in the integrator to filter out the high frequency random current noise and thus the output frequency random jitter can be attenuated.

B. Noise Analysis of Light-to-Frequency Generator

The frequency noise distribution of a typical light-to-frequency converter chip, in root-mean-square (RMS), is simulated with enabling the transient noise option at a 50-kHz converted pulse frequency, which considers the full chip and part-circuit-only noise contributions, respectively. As summarized in Fig. 2, the full chip RMS noise frequency is about 200 Hz, where the photocurrent (PC) buffer contributes most of the noise (170 Hz), and eventually it concludes that the amplifier A_1 inside the photocurrent buffer dominates the whole chip noise performance (150 Hz).
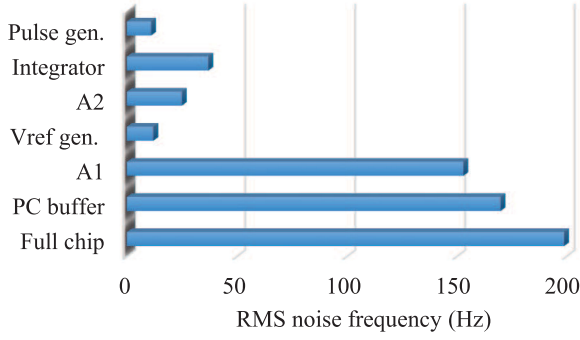
Fig. 2. Noise distribution of a typical light-to-frequency converter chip when a 50-kHz converted pulse frequency F_{osc} is generated. Amplifier A_1 dominates the photocurrent (PC) buffer noise as well as the total noise.

Fig. 4. Concept diagram of the output pulse frequency quantization noise induced by limited operating frequency of MCUs.
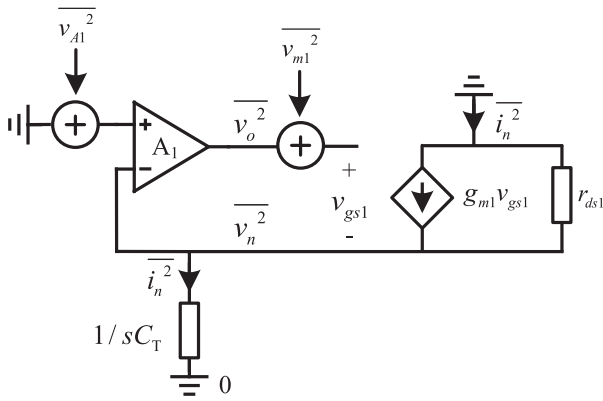

Fig. 3. Noise model of the photocurrent buffer including the amplifier A_1, transistor M_1, and the total parasitic capacitor C_T.

Fig. 3 shows the noise model of the photocurrent buffer including the amplifier A_1, the long-channel NMOS transistor M_1 and the total parasitic capacitor C_T (including the photodiode capacitance in the level of hundred pF and the input capacitance of the amplifier), where $\overline{v_{A1}^2}$ and $\overline{v_{m1}^2}$ are the input-referred voltage noise power spectre density (PSD) of A_1 and M_1, respectively. Using a PMOS transistor to implement M_1 is difficult, since it changes V_n into a high impedance node and the fast-tracking sensing feature is degraded. With a negative feedback configuration, the output small signal of the amplifier is directly fed back into the inverting-input through the voltage buffer M_1, where M_1 provides a 30-kHz bandwidth under a 500-nA photocurrent. In practice, the voltage noise power of V_o is much larger than the voltage noise at V_n, while the noise current in r_{ds} branch is much smaller than the transconductance branch, then the small signal model can be simplified as expressions shown in Eq. (1) and as a result, the output current noise PSD $\overline{i_n^2}$ can be eventually derived as Eq. (2). According to the expression, there are two methods can theoretically optimize the output current noise. At first, decreasing the total parasitic capacitance C_T can significantly reduce the overall output current noise. However, a smaller C_T implies a size shrinkage of the photodiode, which leads to less light-intensity sensitivity. Secondly, ideally if the amplifier bandwidth is infinity large, 4kT/(gm.A_1^2)
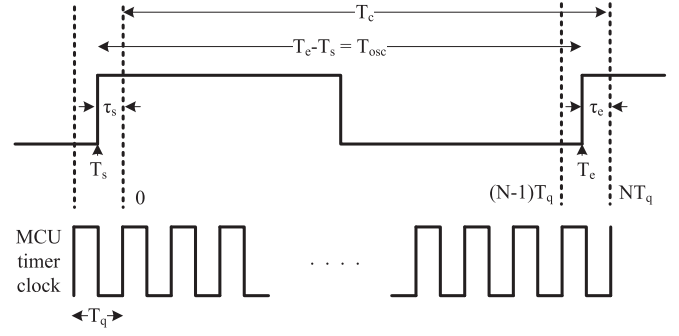
noise component in Eq. (1) can be ignored. However, due to the limited gain-bandwidth product (GBW) of A_1 for a low-power design, the noise PSD introduced by M_1 becomes significant at high-frequency region. Therefore, increasing the amplifier GBW is an important method to reduce the output current noise density, especially at high-frequency region. On the other hand, the noise in low-frequency region (where gain of A_1 is very large) is determined by $s^2 C_T^2 \overline{v_{A1}^2}$. Thus, decreasing C_T and $\overline{v_{A1}^2}$ can efficiently reduce the output current noise power in low-frequency region.

$$
\begin{cases}
\overline{i_n^2} = g_{m1}^2 \left[\left(\overline{v_{A1}^2} - \overline{v_n^2} \right) A_1^2 + \overline{v_{m1}^2} \right] \\[2mm]
\overline{v_n^2} = \dfrac{\overline{i_n^2}}{s^2 C_T^2}
\end{cases}
\tag{1}
$$

$$
\overline{i_n^2} = \frac{g_{m1}^2 \overline{v_{A1}^2} A_1^2 + \frac{2}{3} 4kT g_{m1}}{1 + \dfrac{1}{s^2 C_T^2} g_{m1}^2 A_1^2}
\tag{2}
$$

C. Noise Analysis of Pulse Frequency Quantizer

The output frequency F_{osc} of the light-to-frequency converter can be quantized by timer counting in the following MCU. Fig. 4 depicts the concept diagram of the output pulse frequency quantization noise induced by limited operating frequency in the timer. Assuming that the rising edge of the input signal is T_s and the next rising edge is T_e, the actual period of F_{osc} can be defined by Eq. (3).

$$
T_{\text{osc}} = T_e - T_s
\tag{3}
$$

$$
T_c = T_{\text{osc}} - \tau_s + \tau_e = N T_q
\tag{4}
$$

However, due to the timer quantization noise, the measured period of the pulse signal T_c could be expressed in Eq. (4), where τ_s and τ_e are the quantization noise introduced by the timer. Assuming that τ_s and τ_e are uniformly distributed in the ranges of $(-T_q, 0]$ and $[(N-1) T_q, N T_q)$, respectively, the mean-squared noise power of the measured period can be calculated as Eq. (5).

$$
\overline{\tau_s^2} = \overline{\tau_e^2} = \frac{1}{T_q} \int_0^{T_q} x^2 \, \mathrm{d}x = \frac{1}{3} T_q^2
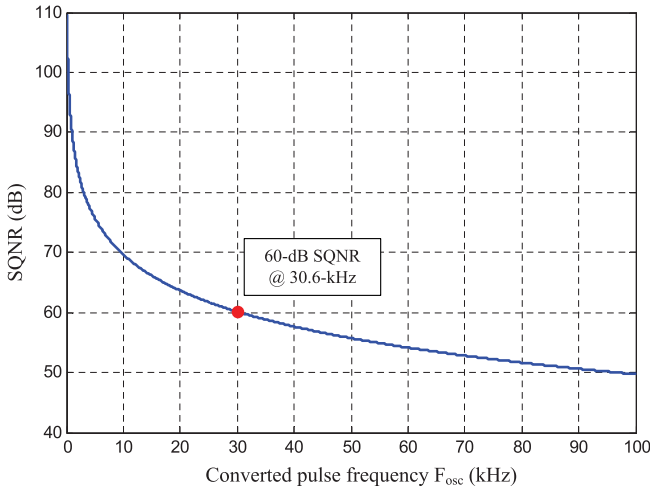\tag{5}
$$

Fig. 5. Simulated signal-to-quantization-noise-ratio (SQNR) as a function of the converted pulse frequency from light at a MCU timer clock of 25-MHz frequency.

Then, the signal-to-quantization-noise ratio (SQNR) of the quantized period could be estimated according to the powers of measured period and quantization noise. In practice, the obtained SQNR is expected to be higher than a minimum value and because the smaller the period T_{osc}, the more significant the quantization noise, the minimum SQNR can be derived as Eq. (6). The relationship between SQNR and the pulse frequency signal is illustrated in Fig. 5, at a typical timer clock of 25 MHz for portable oximeter devices. If the minimum SQNR requirement is 60 dB, the frequency of the input signal must be limited within 30.6 kHz, and when the quantization noise requirement is increased to 65 dB, the input signal should be limited within 17.2 kHz.

$$\mathrm{min(SQNR)} = \frac{\mathrm{min}(T_{osc}^2)}{2 \cdot T_q^2/3} = \frac{3}{2}\left[\frac{F_q}{\mathrm{max}(F_{osc})}\right]^2 \qquad (6)$$

III. PROPOSED LOW-NOISE LIGHT-TO-FREQUENCY CONVERTER SCHEME

A. Proposed Low-Noise Photocurrent Buffer Scheme

Fig. 6 shows the transistor-level schematic of the proposed photocurrent buffer, using a g_m-boost operational amplifier A_1 that can efficiently reduce noise. The fundamental circuit structure of the amplifier is folded-cascode with P-type differential input-pair. Considering the induced stability issue due to the high gain A_1, the PMOS part in the load impedance does not have a cascode structure. On the contrary, the NMOS part in the load impedance requires the cascode structure in order to ensure that the drain voltage of $M_{10/11}$ is clamped near 300 mV to guarantee a zero volt input common-mode voltage. By mirroring the bias current to M_{15} branch, the reference voltage V_{bn2} can be generated through a long channel transistor M_{16} to provide a DC bias for $M_{8/9}$. The proposed g_m-boost circuit is illustrated inside the red dashed box in Fig. 6. The bias current flowing through M_{14} generates a reference voltage V_{bn1} to set DC operating points of M_{10} and M_{11} through two R_b resistors,

respectively. In order to improve the AC transconductance of A_1, two C_b capacitors are introduced to connect differential inputs and gates of $M_{10/11}$. At high-frequency region, the AC-part of V_{in} is superposed in the gate of $M_{10/11}$ and as a result, a larger equivalent g_m is obtained, as shown by the AC-gain definition in Eq. (7). According to the transistor voltage noise model [15], the amplifier output noise can be efficiently reduced if the input-stage g_m at the high-frequency region is increased. It worth to be noted that, since there is no static current in R_b, the DC operating point of A_1 has no change when compared with traditional folded-cascode amplifier, which implies that the proposed g_m-boost amplifier costs extra chip area but consumes no additional power.

$$A_{v1} = \left(g_{m2} + \frac{sR_bC_b}{1 + sR_bC_b}g_{m10}\right)r_{ds5} \qquad (7)$$

According to the simulation result, for the frequency region below 3 kHz, the proposed g_m-boost scheme has no effect on noise reduction, because the capacitor C_b can be seen as an open circuit and the 1/f noise dominates the total noise in low frequency. At the range of 3 kHz to 250 kHz, the proposed scheme increases the noise PSD because of the introduced resistor R_b. At the high frequency range beyond 250 kHz, the noise PSD is effectively attenuated due to the extended bandwidth. The total integrated noise from 100 Hz to 1 MHz is reduced from 1.36 mVrms to 1.05 mVrms, showing more than 22% improvement. Higher frequency noise is not taken into account in this work, which is low-pass filtered during the photocurrent integration. At high temperature of 85 °C, the noise reduction of 18% is also verified.

B. Proposed Output Pulse-Frequency-Duty-Cycle Modulation Scheme

Traditionally, F_{osc} is the divided-by-2 converted pulse frequency with 50% duty cycle, as shown in Fig. ??. In order to limit the maximum F_{osc} for higher SQNR, a digital processing unit with pulse-frequency-duty-cycle modulation scheme is proposed. The basic idea of this technique is to map the output pulse duty cycle when F_{osc} exceeds a certain threshold frequency, and thus it significantly extends the sensing dynamic range while a high frequency output can be avoided. As shown by the schematic in Fig. 7, F_{osc} is at first transformed into four binary-scaled output frequencies F_{o1-4} with different duty cycles of 50%, 75%, 62.5% and 37.5%, respectively. Then, the second digital block selects one of the four output signals according to the comparison result with the reference frequency F_{ref}, as expressed in Eq. (8). For instance, the F_{o1} is selected as the final output F_{out} when the frequency of F_{osc} is less than 1/16 of the F_{ref} frequency and Fout is equal to F_{o4} if F_{osc} is larger than $F_{ref}/4$. The proposed digital processing unit output frequency and its duty cycle as a function of F_{osc}, as normalized to the reference frequency F_{ref}, are shown in Fig. 8. The output multiplexer function is fully implemented in digital domain and relies on the introduced stable reference frequency F_{ref}, which is generated on-chip with insensitive characteristics to process and
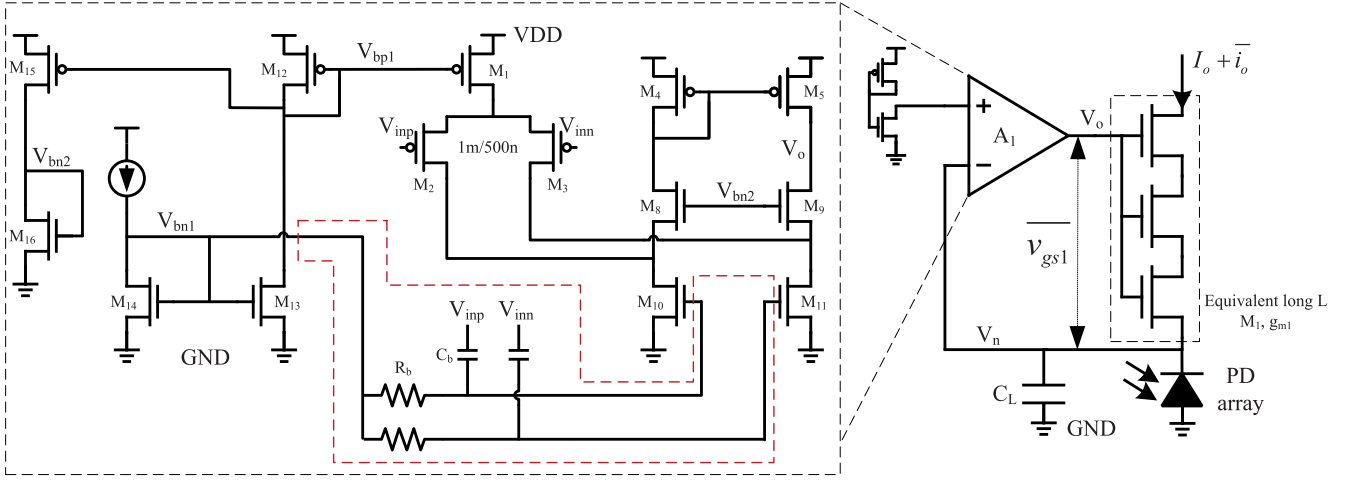
Fig. 6. Transistor-level schematic of the proposed g_m-boost low-noise operational amplifier A_1 inside the photocurrent buffer unit.

environmental temperature variations. Moreover, a hysteresis-comparison mechanism should be adopted during the frequency selection progress to avoid output frequency fluctuation.

$$F_{\text{out}} = \begin{cases} F_{o1} & F_{\text{osc}} < F_{\text{ref}}/16 \\ F_{o2} & F_{\text{ref}}/16 \leq F_{\text{osc}} < F_{\text{ref}}/8 \\ F_{o3} & F_{\text{ref}}/8 \leq F_{\text{osc}} < F_{\text{ref}}/4 \\ F_{o4} & \text{otherwise} \end{cases} \quad (8)$$

The maximum output frequency of F_{out} can be expressed by Eq. (9). If the frequency of F_{osc} is less than $F_{\text{ref}}/4$, F_{out} is no larger than $F_{\text{ref}}/32$. Otherwise, F_{out} is equal to F_{o4}. In order to guarantee the maximum frequency of F_{out} is 30.6 kHz for 60-dB SNQR under 25-MHz timer clock, the converted pulse frequency F_{osc} should be limited below 489.6 kHz, while F_{ref} is designed to be around 979.2 kHz.

$$\max(F_{\text{out}}) = \begin{cases} F_{\text{ref}}/32 & F_{\text{osc}} < F_{\text{ref}}/4 \\ F_{\text{osc}}/16 & \text{otherwise} \end{cases} \quad (9)$$

C. Proposed Process-Insensitive Reference Frequency Source

The transistor-level schematic of the proposed process-insensitive reference frequency source F_{ref} is given in Fig. 9, which is composed of the compensation circuit and the ring oscillator. In this work, an around 1-MHz reference frequency is expected, operating from -25 to 85-°C environmental temperature and across three main process corners [16] for the aim of 90% wafer yield. The 2.2-V power supply for this circuit can be generated from an on-chip voltage regulator.

The compensation circuit creates a process-dependent reference voltage by using a threshold-voltage (V_T) sensing technique. The left part of Fig. 9 is a bandgap reference that provides a proportional-to-absolute-temperature (PTAT) current I_b for the V_T sensing. Different from the previous design [17], the proposed circuit can avoid using an operational amplifier. As

derived in Eq. (10), V_b dependent on V_{ref} which can be generated from the internal bandgap reference circuit. According to the Spice model, when process corner increases from typical to fast-fast (ff), the transistor V_T decreases and the electron mobility increases, leading to larger V_b. Similarly, V_b decreases if the CMOS process changes to slow-slow (ss) corner. This process-dependent reference voltage is adopted to bias the following ring-oscillator.

$$V_b = Vdd - Vth_6 - \sqrt{\frac{2V_T \log N}{\mu_n C_{ox} R_{b1} (W/L)_{b6}}} \quad (10)$$

The reference frequency is generated using a ring-oscillator with three stages delay elements and each one uses the simple inverter structure to minimize the process variation. The output reference frequency of this oscillator is given in Eq. (11), where C_0 is the total load capacitance of each delay element. V_{swing} is the output voltage swing. The key to generating a constant output frequency is to get an accurate current with temperature and process independence. Since V_b and the self-excited oscillator frequency have inverse coefficients of the process corner and temperature, the output frequency F_{ref} can be compensated and just remains a small residual variation. Fig. 10 shows the simulated 1-MHz F_{ref} with the proposed compensated ring-oscillator structure under different process corners and temperatures, which indicates that the frequency variation is able to keep within 5% in the range of -25 to 85 °C.

$$F_{\text{ref}} = \frac{\mu_n C_{ox} W}{L} \frac{(Vdd - V_b - Vth_{r1})^2}{6C_0 V_{\text{swing}}} \quad (11)$$

IV. MEASUREMENT RESULTS

A. Light-to-Frequency Converter Chip Measurement Result

The proposed light-to-frequency converter chip is implemented and fabricated using 0.35-μm CMOS process. Fig. 11 shows the chip microphotograph. The total chip area is about $1 \times 0.9 \text{ mm}^2$ with on-chip 7×7 Nwell-Psub photodiode array which are shorted in parallel. About 24000 dies in each 8-inch wafer
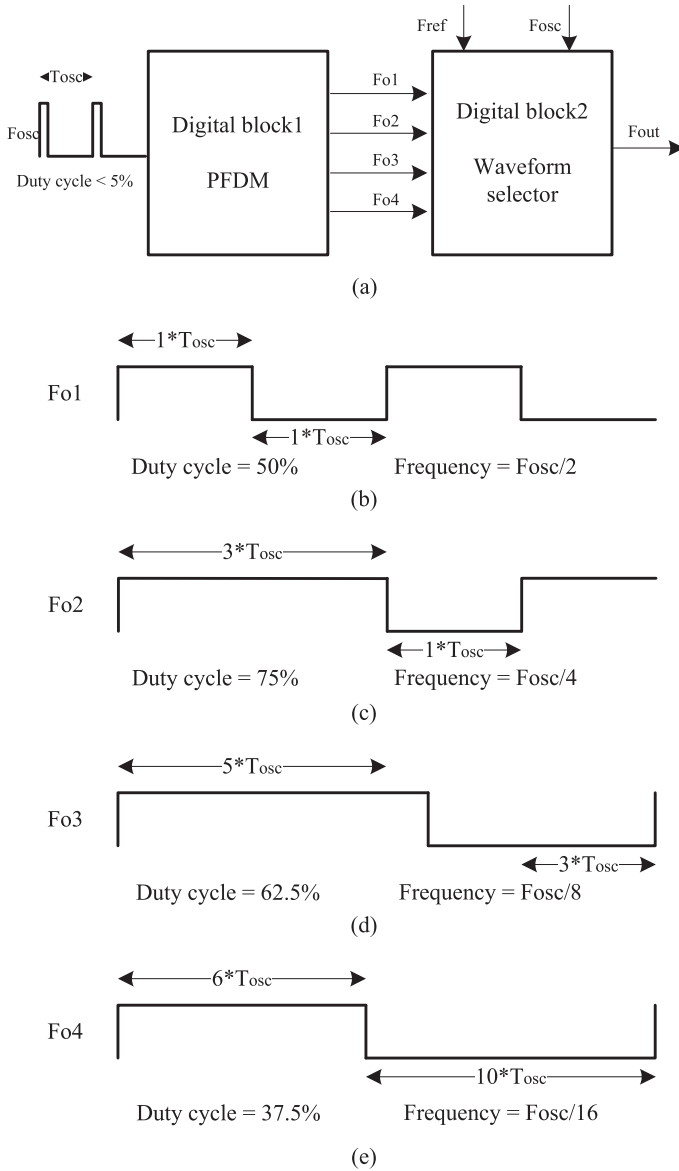
Fig. 7. Digital processing schematic of the proposed pulse-frequency-duty-cycle modulation scheme.

Fig. 8. Digital processing unit output frequency F_{out} (a) and its duty cycle (b) as a function of the converted pulse frequency F_{osc} normalized to the reference frequency F_{ref}.

Fig. 9. Transistor-level schematic of the proposed process-insensitive 1-MHz reference frequency source for F_{ref} generation with compensated ring-oscillator structure.

using 80-μm standard scribe line width is able to be produced and the yield is about 91%. A colorless resin package is adopted with a side-looker lens and 98% transparency [18]. The wafer-level measurement for verifying the process variation is performed by testing the output frequency deviations under a typical condition of 20-kHz mean output frequency. According to Fig. 12, the normalized output frequency variations are between +5% and −4% with approximately Gaussian distribution.

The intrinsic noise performance of the proposed chip is characterized by measuring the frequency jitter of F_{osc} using a Keysight oscilloscope MSO9254A. Fig. 13 shows the measurement setup. A stable LED light source and a light integrating sphere are adopted when testing the chip performance. As shown in Fig. 14, the typical random jitter frequency of the proposed light-to-frequency converter at 100-kHz output is about 156 Hz
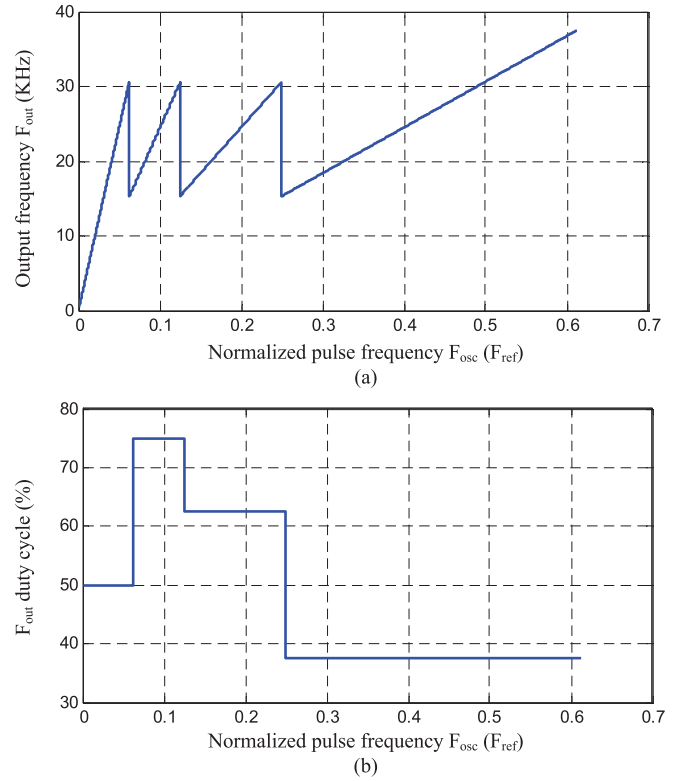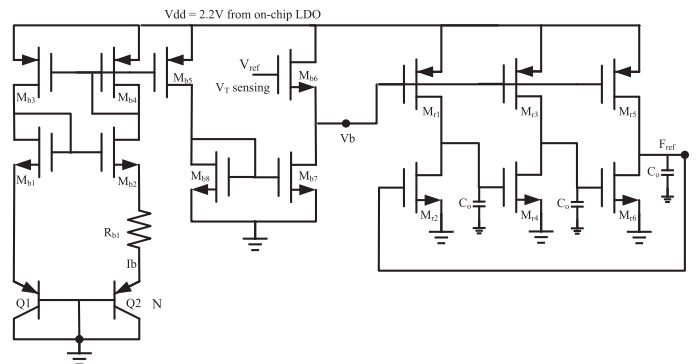
in standard deviation (referring to a 56.1-dB SNR), which is calculated with about 1000 continuous output cycles, while the peak-to-peak frequency deviation is about 1.24%. The measured SNR results of F_{osc} as a function of its frequency from 50 Hz to near 1 MHz is illustrated in Fig. 15. According to the comparison between the proposed design (blue line) and the previous design (red line), the peak SNR is about 60 dB and a 9-dB SNR improvement is achieved at 10-kHz typical output oscillation frequency, which is expectedly benefited from three aspects: first, the proposed low-noise photocurrent buffer reduces the output random jitter noise of about 3 dB; second, the transistor
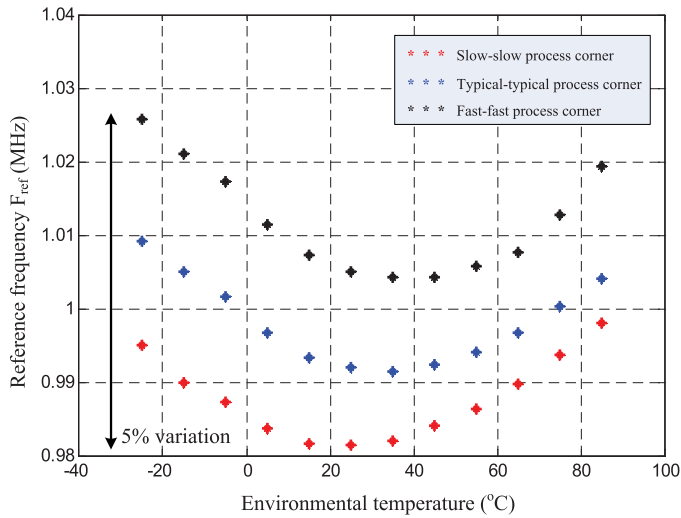
Fig. 10. Simulated 1-MHz reference frequency source output $F_{\rm ref}$ as a function of the environmental temperature in different process corners, 5% frequency variation is verified.
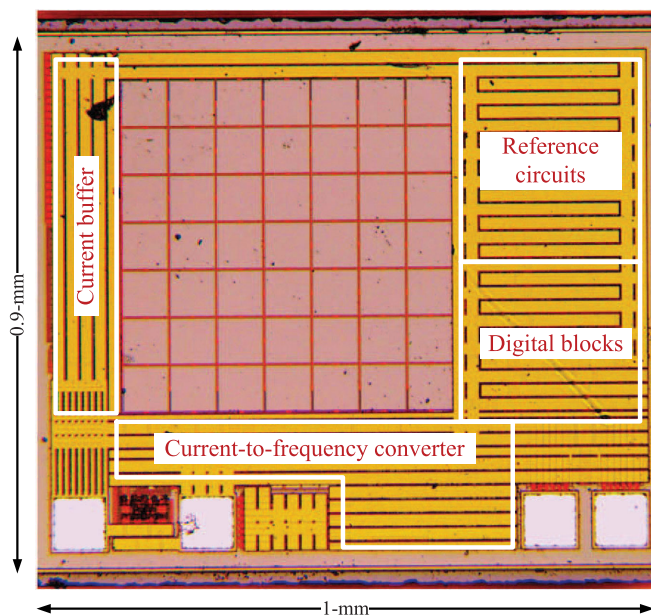

Fig. 12. Measured normalized output frequency deviations among 24000 dies in a wafer with 20-kHz mean frequency.

Fig. 11. Fabricated chip microphotography of the proposed g_m-boost low noise light-to-frequency converter with 1×0.9-mm^2 die size.

Fig. 13. The measurement setups for the chip testing using light integration sphere and the blood SpO$_2$ sensing system testing.

Fig. 14. Measured transient output $F_{\rm osc}$ waveform at 100-kHz frequency with 156-Hz standard deviation jitter noise.

width of the input-differential pair in the photocurrent buffer is increased from previous 300 μm to 1 mm (with the same 500-nm transistor length) to reduce the flicker noise; third, the layout of this work is improved compared with the previous design with a larger decoupling capacitor and grounded guard-ring for each analog unit. It shows the previous design has smoother SNR response than the proposed design, which implies that the environmental interference light during the chip test causes the noise change since the proposed design has much smaller noise floor.

The functionality is proven by measuring the transient waveforms of both $F_{\rm osc}$ and $F_{\rm out}$. As shown in Fig. 16, the original
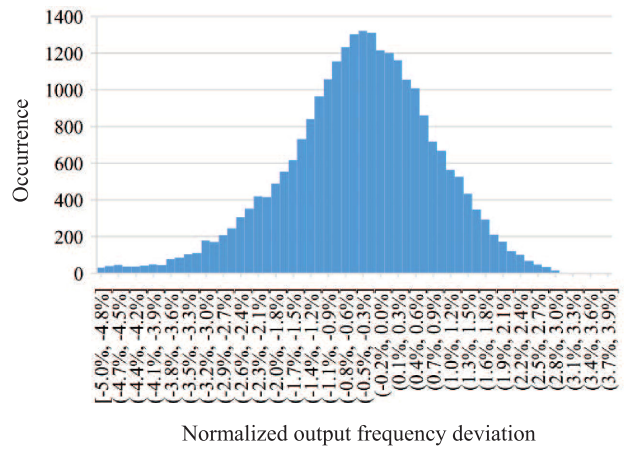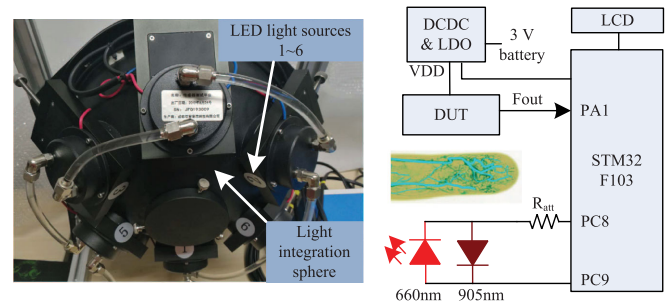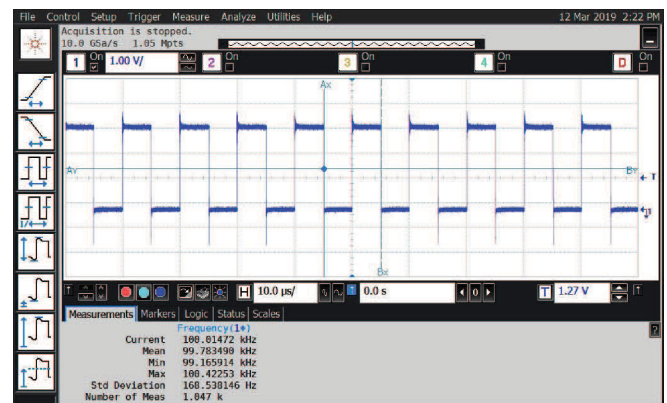
pulse frequency $F_{\rm osc}$ (upper line) is 500 kHz with 50% duty cycle, while the modulated final output frequency $F_{\rm out}$ (lower line) becomes 37.5% duty cycle. The random jitter is reduced from 1 kHz to only 13.7 Hz due to the low-pass filtering effect benefiting from the digital frequency divider, which refers to an output SNR of 66 dB increasing from 54 dB as indicated by the
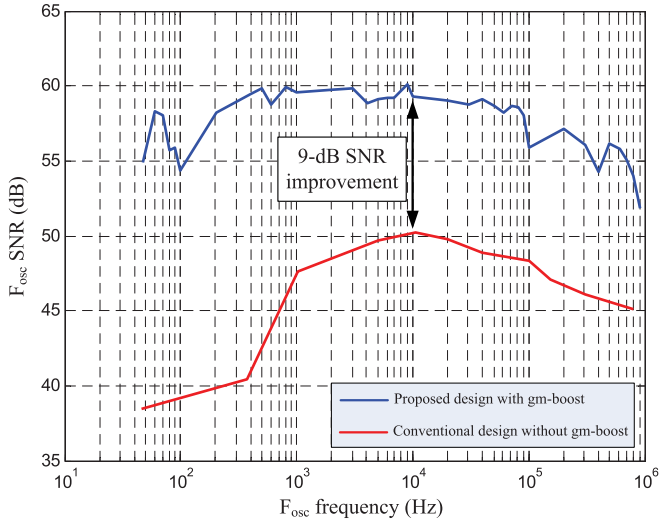
Fig. 15. Measured F_{osc} SNR results as a function of its frequency for both the proposed design (blue line) and the previous design (red line), respectively. A 9-dB SNR improvement is achieved at 10-kHz typical output oscillation frequency.
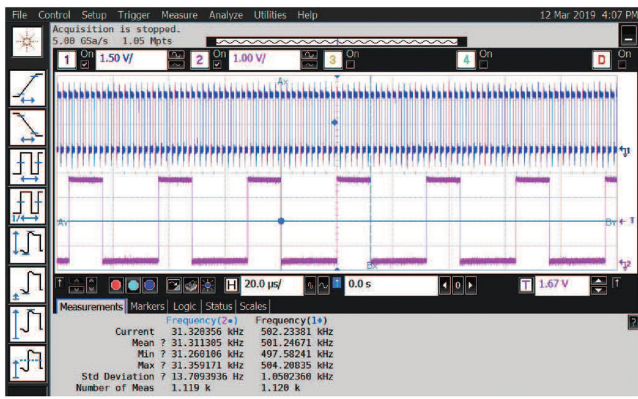

Fig. 17. Measured SNR of F_{osc} as a function of the power supply voltage from 2.4 to 3.3 V.

Fig. 16. Measured transient output waveforms for 500 kHz 50% duty cycle F_{osc} (upper line) and divided-by-16 final output frequency 37.5% duty cycle F_{out} (lower line), as well as their standard deviation jitter results, proving a significant noise reduction.
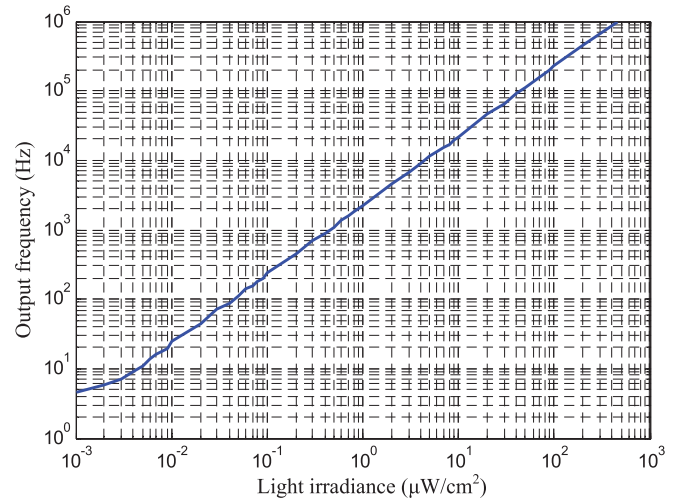
Fig. 18. Measured output frequency dynamic range as a function of the incident light irradiance.

SNR improvement expression in Eq. (12).

$$\mathrm{SNR}_{\mathrm{inc}} = 10 \log \left(\frac{F_{\mathrm{osc}}}{F_{\mathrm{out}}} \right) \quad (12)$$

The noise performance as a function of the power supply voltage from 2.4 to 3.3 V is measured, as shown in Fig. 17. When the supply voltage is larger than 2.6 V, output SNR is almost constant above 53.5 dB. As the power supply becomes below 2.6 V, for example because of battery-low, the obtained signal quality obviously deteriorates and the 1-dB SNR voltage corner happens at 2.4 V, where the SNR drop at lower power supply is mainly due to the limitation of amplifier's operating voltage range. Since the adopted transistors in this work are 5-V thick-gate-oxide types, the acceptable operating supply voltage covers the range from 2.4 to 5.5 V. The output frequency dynamic range is measured under different incident light irradiance at
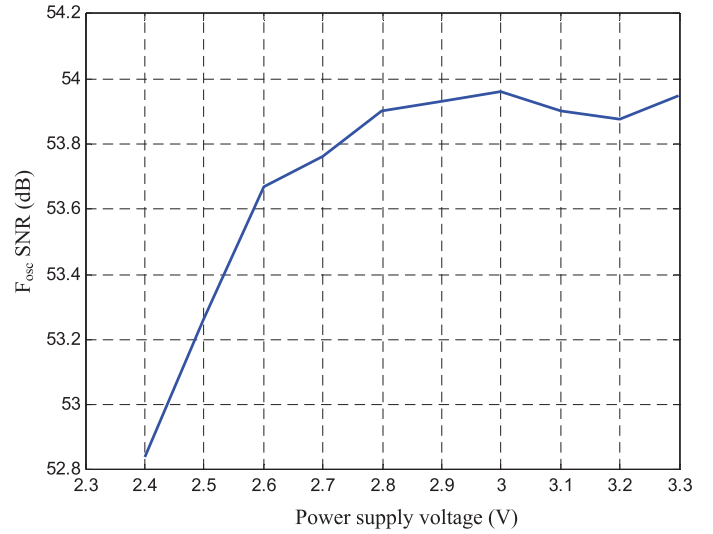
room temperature, as shown in Fig. 18. It indicates that the output linear range covers from 10 Hz to 1 MHz, which refers to 100-dB linear dynamic range of the output frequency. Table I summarizes the detailed performance of the proposed chip and the reference designs. The additional current consumption and chip area due to the proposed design are is 12% and 15%, respectively.

B. Blood SpO$_2$ Sensing System Measurement Result for Hypoperfusion Applications

To implement a portable blood oximeter prototype, a typical 3-V battery voltage source is firstly boosted and then linearly regulated down to 3.3-V supply for both the MCU and the proposed device-under-test (DUT). Both 660-nm red and 905-nm infrared LED light sources are used in parallel, while the LED

TABLE I
SUMMARY AND COMPARISON OF THE LIGHT-TO-FREQUENCY CONVERTER CHIP MEASUREMENT RESULTS

SPECIFICATION	T-ED 2016 [7]	T-BIOCAS 2019 [16]	T-ED 2013 [19]	J-SSC 2014 [20]	Sensors [22]	ISSCC 2017 [23]	SENSOR J. [24]	THIS WORK
CMOS Process	350 nm	350 nm	180 nm	180 nm	180nm	180nm	700nm	350 nm
Supply Voltage	2.5 V~5.5 V	2.5 V~5.5 V	1.2 V/2.5 V	0.5 V	3.3V	0.15V~0.36V	3.3 V	2.4 V~5.5 V
Operating Temp.	-40~125ºC	-25~80ºC	---	Up to 70 ºC	-40~125 ºC	-20~80 ºC	---	-25~85ºC
Supply Current	0.5 mA	1.9 mA @500kHz Fo 0.7 mA @25kHz Fo	---	8 μA	---	<3.6nA	0.3 mA	1.6~1.8 mA
Sensitivity	550 Hz/μW/cm^2	2.2 kHz/μW/cm^2	85 Hz/lux	4 nA	1.15 μA/lux	---	280 Hz/nA	2.2 kHz/μW/cm^2
Dynamic Range	Linear 126 dB	Linear 100 dB	124 dB	58 dB	---	>140dB	---	Linear 100 dB
SNR @ 500kHz Fo	---	39 dB	---	---	50.5dB~ 52.64dB	---	---	54dB before modulating 66dB after modulating
Step Response Settling Cycles	>= 10 cycles	<=2 new cycles	---	---	---	---	---	<=2 new cycles
Temperature Co.	---	+/-205 ppm/°C	---	---	---	---	---	+/-200 ppm/°C
ΔFo @2.7V~5.5V	+/-1%	+/-1%	---	---	---	---	---	+/-1%
Chip area (mm^2)	1.02 x 0.83	1 x 0.9		1.63 x 1.63	0.76 x 0.45	1 x 1	0.25 x 0.07	1 x 0.9

switching is realized by controlling the flowing direction of the LED current. An industrial 32-bit ARM Cortex-M3 MCU is used for photoplethysmography (PPG) signal procession and LED driving. A resistor R$_{att}$ in-series is adopted to attenuate the LED current, thus the emitting light intensity can be controlled according to the resistance. To verify the micro-system functionality of the blood SpO$_2$ sensor using the proposed light-to-frequency converter, a Fluke index 2 pulse oximeter tester is adopted as the golden standard [21]. The SpO$_2$ error as a function of the golden standard SpO$_2$ is measured, under conditions of 3% PI, 75-bpm PR and 0.1% PI, 75-bpm PR, respectively, as demonstrated in Fig. 19.a, which proves that the measured SpO$_2$, in the range from 40% to 100%, has an absolute sensing error within 1-percentage-point. The pulse rate can also be correctly sensed by the proposed light-to-frequency converter chip with an absolute sensing error of 1 bpm, under conditions of 96% SpO$_2$, 3% PI and 96% SpO$_2$, 0.1% PI, respectively, as shown in Fig. 19(b).

In order to estimate the minimum measurable perfusion index condition, two experiments are carried out. First, the SpO$_2$ error as a function of perfusion index is measured as shown in Fig. 20(a), under 75-bpm pulse rate and different SpO$_2$ conditions of 30%, 60% and 90%, respectively, which proves that the absolute SpO$_2$ sensing error is within 2-percentage-point while the minimum measurable perfusion index condition is 0.06%. Second, the SpO$_2$ error as a function of perfusion index, under 90% SpO$_2$ and different pulse rate conditions of 30 bpm, 120 bpm and 250 bpm, respectively, is measured as shown in
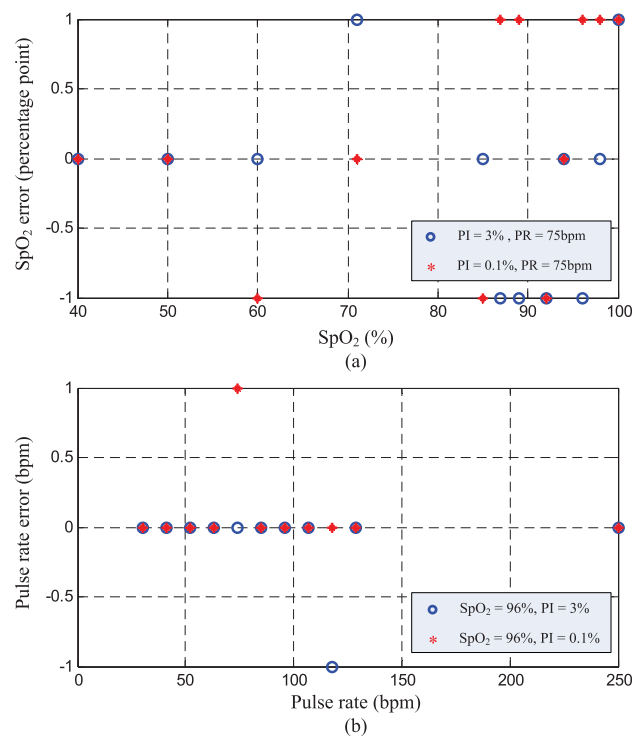

Fig. 19. Measurement results of: (a) SpO$_2$ errors as a function of the golden standard SpO$_2$ under conditions of PI = 3%, PR = 75 bpm and PI = 0.1%, PR = 75 bpm, respectively; (b) pulse rate errors as a function of the golden standard pulse rate under conditions of SpO$_2$ = 96%, PI = 3% and SpO$_2$ = 96%, PI = 0.1%, respectively.
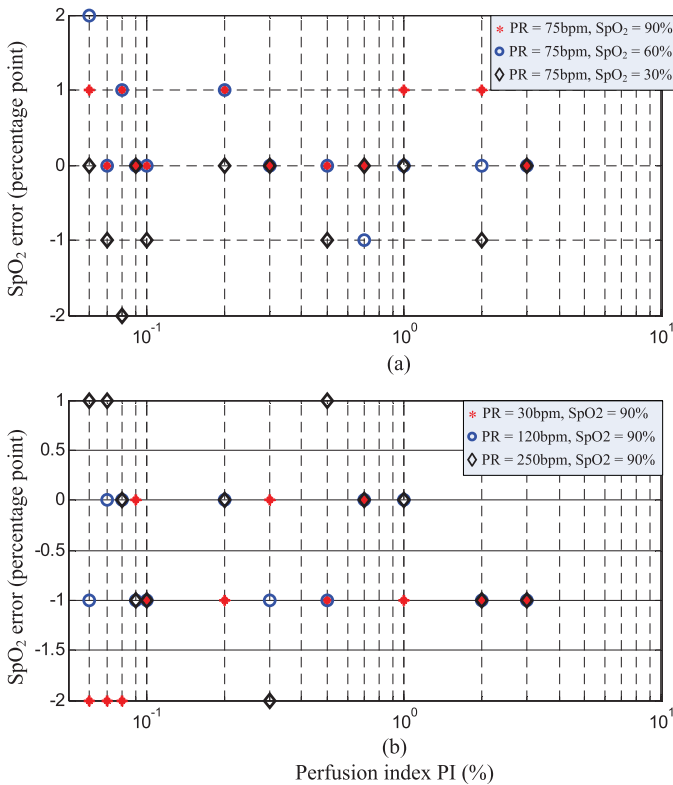
Fig. 20. Measurement results of (a) SpO_2 errors as a function of perfusion index, under different SpO_2 conditions of 30%, 60% and 90%, respectively. Minimum measurable perfusion index condition of 0.06% is proved and (b) SpO_2 errors as a function of perfusion index, under different pulse rate conditions of 30 bpm, 120 bpm and 250 bpm, respectively. Minimum measurable perfusion index condition of 0.06% is proved.

Fig. 20(b), which proves that the SpO_2 sensing error is within -2 to 1-percentage-point while the minimum measurable perfusion index condition is also 0.06%. The sensing results under lower perfusion index condition are unstable. If the PI condition is lower than 0.02% such as medical treatments for pets or infants, the sensor SNR should be higher than 90 dB, which can be realized by a high resolution $\Sigma\Delta$ ADC.

V. CONCLUSION

This paper presents a low-noise light-to-frequency sensor. Two noise reduction techniques are introduced that are low-noise photocurrent buffer with transconductance-boost (g_m-boost) circuit structure and digital frequency limiter using pulse-frequency-duty-cycle modulation. The proposed light-to-frequency sensor chip is silicon-proven with 0.35-μm CMOS process and the overall chip area is 1×0.9 mm^2 while the total current consumption is 1.8 mA from a 3.3-V power supply. The measurement results show that the SNR of a typical output frequency increases from 50 dB to 59 dB while the frequency divider can contribute an additional 12-dB peak SNR improvement. For the 9-dB improvement, 2-3 dB stem from the gm-boosting and the other 6dB from improvements in layout that are standard practice. The additional current consumption

and chip area are 12% and 15%, respectively. In-system experimental results show that the minimum measurable PI using the proposed blood SpO_2 sensor could be as low as 0.06%, which shows the advancement for portable sub-0.1% hypoperfusion blood oximeter applications.

REFERENCES

[1] J. Xu et al., "A 36 μW 1.1 mm^2 reconfigurable analog front-end for cardiovascular and respiratory signals recording," IEEE Trans. Biomed. Circuits Syst., vol. 12, no. 4, pp. 774–783, Aug. 2018.

[2] S. Sinchai, P. Kainan, P. Wardkein and J. Koseeyaporn, "A photo-plethysmographic signal isolated from an additive motion artifact by frequency translation," IEEE Trans. Biomed. Circuits Syst., vol. 12, no. 4, pp. 904–917, Aug. 2018.

[3] J. Lee, D. Jang, S. Park, and S. Cho, "A low-power photoplethysmogram-based heart rate sensor using heartbeat locked loop," IEEE Trans. Biomed. Circuits Syst., vol. 12, no. 6, pp. 1220–1229, Dec. 2018.

[4] J. A. C. Patterson and G.-Z. Yang, "Ratiometric artifact reduction in low power reflective photoplethysmography," IEEE Trans. Biomed. Circuits Syst., vol. 5, no. 4, pp. 330–338, Apr. 2011.

[5] S. V. Gubbi and B. Amrutur, "Adaptive pulse width control and sampling for low power pulse oximetry," IEEE Trans. Biomed. Circuits Syst., vol. 9, no. 2, pp. 272–283, Apr. 2015.

[6] M. Shokouhian, R. Morling, and I. Kale, "Interference resilient sigma delta-based pulse oximeter," IEEE Trans. Biomed. Circuits Syst., vol. 10, no. 3, pp. 623–631, Mar. 2016.

[7] F. Tang et al., "A linear 126-dB dynamic range light-to-frequency converter with dark current suppression upto 125°C for blood oxygen concentration detection," IEEE Trans. Electron Devices, vol. 63, no. 10, pp. 3983–3988, Oct. 2016.

[8] R. G. Correia, S. Pimenta and G. Minas, "CMOS integrated photodetectors and light-to-frequency converters for spectrophotometric measurements," IEEE Sensors J., vol. 17, pp. 3438–3445, 2017.

[9] D. Mishra, S. Chandra, A. Chandra, S. Jain, and M. Sarkar, "A portable system for real-time non-contact blood oxygen saturation measurements," in Proc. IEEE Biomed. Circuits Syst. Conf., 2017, pp. 1–4.

[10] L. Turicchia et al., "Ultra low-power electronics for cardiac monitoring," IEEE Trans. Circuits Syst. I, Reg. Papers, vol. 57, no. 9, pp. 2279–2290, 2010.

[11] G. Ryu et al., "Flexible and printed PPG sensors for estimation of drowsiness," IEEE Trans. Electron Devices, vol. 65, no. 7, pp. 2997–3004, Jul. 2018.

[12] M. Tavakoli, L. Turicchia, and R. Sarpeshkar, "An ultra-low-power pulse oximeter implemented with an energy-effcient transimpedance amplifier," IEEE Trans. Biomed. Circuits Syst., vol. 4, no. 1, pp. 27–38, Feb. 2010.

[13] H. Lee, H. Ko, C. Jeong, and J. Lee, "Wearable photoplethysmographic sensor based on different LED light intensities," IEEE Sensors J., vol. 17, no. 3, pp. 587–588, Feb. 2017.

[14] K. Li, S. Warren, and B. Natarajan, "Onboard tagging for real-time quality assessment of photoplethysmograms acquired by a wireless reflectance pulse oximeter," IEEE Trans. Biomed. Circuits Syst., vol. 6, no. 1, pp. 54–63, Feb. 2012.

[15] G. Mulberry, K. A. White, and B. N. Kim, "Analysis of simple half-shared transimpedance amplifier for picoampere biosensor measurements," IEEE Trans. Biomed. Circuits Syst., vol. 13, no. 2, pp. 387–395, Feb. 2019.

[16] F. Tang et al., "A low power and fast tracking light-to-frequency converter with adaptive power scaling for blood SpO_2 sensing," IEEE Trans. Biomed. Circuits Syst., vol. 13, no. 1, pp. 26–37, Jan. 2019.

[17] K. Sundaresan and P. E. Allen, "Process and temperature compensation in a 7-MHz CMOS clock oscillator," IEEE J. Solid-State Circuits, vol. 41, no. 2, pp. 433–442, Feb. 2006.

[18] Texas Advanced Optoelectronic Solutions Inc. (TAOS), "TSL237R light-to-frequency converter datasheet," 2007. [Online]. Available: http://ams. com/eng/ Products/Light-Sensors/Light-to-Frequency/TSL237

[19] T.-H. Tsai, and R. Hornsey, "A quad-sampling wide-dynamic-range pulse-frequency modulation pixel," IEEE Trans. Electron Devices, vol. 60, no. 2, pp. 805–811, Feb. 2013.

[20] M. Alhawari, N. Albelooshi, and M. H. Perrott, "A 0.5 V $< 4\mu$W CMOS light-to-digital converter based on a nonuniform quantizer for a photo-plethysmographic heart-rate sensor," IEEE J. Solid-State Circuits, vol. 49, no. 1, pp. 271–288, Jan. 2014.

[21] Fluke Index 2XL Users Manual, 2007. [Online]. Available: https://www.flukebiomedical.com/products/biomedical-test-equipment/patient-monitor-simulators/index-2-xlfe-pulse-oximeter-tester?PID=56330

[22] W.-S. Lin, G.-M. Sung, and J.-L. Lin, "High performance CMOS light detector with dark current suppression in variable-temperature systems," *Sensors*, vol. 17, no. 1, pp. 271–288, Jan. 2017.

[23] W. Lim, D. Sylvester and D. Blaauw, "4.4 A sub-nW 80mlx-to-1.26Mlx self-referencing light-to-digital converter with AlGaAs photodiode," in *Proc. IEEE Int. Solid-State Circuits Conf. Dig. Tech. Papers*, 2017, pp. 72–73.

[24] W. Lim, D. Sylvester and D. Blaauw, "4.4 A sub-nW 80mlx-to-1.26Mlx self-referencing light-to-digital converter with AlGaAs photodiode," in *Proc. IEEE Int. Solid-State Circuits Conf. Dig. Tech. Papers*, 2017, pp. 72–73.

Xichuan Zhou, photograph and biography not available at the time of publication.

Shengdong Hu, photograph and biography not available at the time of publication.

Zhi Lin, photograph and biography not available at the time of publication.

Fang Tang (Senior Member IEEE) received the B.S. degree from Beijing Jiaotong University, Beijing, China, in 2006, and the M.Phil and Ph.D degrees from The Hong Kong University of Science and Technology, Hong Kong, in 2009 and 2013, respectively. He is currently the Distinguished Research Fellow with Chongqing University, Chongqing, China, the Associate Director with Chongqing Engineering Laboratory of High Performance Integrated Circuits and leads the Smart Integrated Circuits and Systems Laboratory.

Ping Li received the Ph.D. degree from the University of Electronic Science and Technology of China, Chengdu, China, in 2018. In 2019, he joined Chongqing University, Chongqing, China, where his current research interests include power devices and their applications.
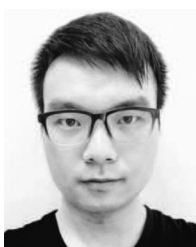

Zhipeng Li received the B.Sc. degree from the College of Electrical Information Engineering, Henan University of Engineering, Henan, China, in 2016. He is currently working toward the master's degree with Chongqing University, Chongqing, China. His current research interest focuses on mixed-signal integrated circuit design for biomedical sensor.

Bo Wang (Member, IEEE) received the B. Eng. degree (with Hons.) in electrical engineering from Zhejiang University (ZJU), Hangzhou, China, in 2010, and the M.Phil. and Ph.D. degrees in electronic and computer engineering from the Hong Kong University of Science and Technology (HKUST), Hong Kong, in 2012 and 2015, respectively.

In 2015, he joined HKUST as a postdoctoral researcher and leaded the HKUST-MIT consortium project on wireless sensing node design for smart green building applications. Afterward, he was with the Massachusetts Institute of Technology in 2016 on low-power data converter design for this project. In 2017, he joined Hamad Bin Khalifa University, Qatar Foundation, as a Founding Faculty, where is currently an Assistant Professor with the Division of Information and Computing Technology, College of Science and Engineering. His current research interests include energy-efficient analog mixed-signal circuits, sensor and sensor interface, and heterogeneous integrated systems for in vitro/vivo health monitoring. Dr. Wang was the recipient of the IEEE ASP-DAC Best Design Award in 2016.
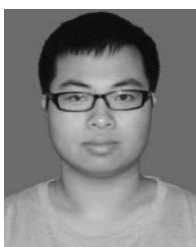
Tongbei Yang received the B.S. degree from the School of Microelectronics and Communication Engineering, Chongqing University, Chongqing, China, in 2017, where he is currently working toward the Ph.D degree, directly from the B.S. degree. His current research interests are mixed-signal integrated circuits design and high frequency analog integrated circuits for telecommunications.

Lai Zhang received the master's degree from the South China University of Technology, Guangzhou, China, in 2007. From 2008, he has been a product manager with R&D department of Guangdong Biolight Meditech Co., Ltd., Zhuhai, China, where he has engaged in research of monitoring parameters of vital signs, such as blood oxygen, electrocardiogram, blood pressure, and so on.
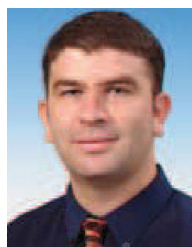
Amine Bermak (Fellow IEEE) received the M.Eng. and Ph.D. degrees in electronic engineering from Paul Sabatier University, Toulouse, France in 1994 and 1998, respectively. He is currently a full Professor with the Department of Electronic and Computer Engineering, The Hong Kong University of Science and Technology (HKUST), Hong Kong. He is also the founder and the leader of the Smart Sensory Integrated Systems Research Lab, HKUST. He was a member of the senate committee with HKUST.